Reemployment of Kupffer's vesicle cells into axial and paraxial mesoderm via transdifferentiation

Takafumi Ikeda[1], Kiichi Inamori[1], Toru Kawanishi[1], Hiroyuki Takeda[1 *]

1 Laboratory of Embryology, Department of Biological Sciences, Graduate School of Science, The University of Tokyo, 7-3-1 Hongo, Bunkyo-ku, Tokyo 113-0033, Japan

*To whom correspondence should be addressed.

Fax: (+81) 3-5841-4434. e-mail: htakeda@bs.s.u-tokyo.ac.jp

Abstract (150-250 words)

Kupffer's vesicle (KV) in the teleost embryo is a fluid-filled vesicle surrounded by a layer of epithelial cells with rotating primary cilia. KV transiently acts as the left-right organizer but degenerates after the establishment of left-right asymmetric gene expression. Previous labelling experiments indicated that descendants of KV-epithelial cells are incorporated into mesodermal tissues after KV collapses (KV-collapse) in zebrafish embryos. However, the overall picture of their differentiation potency had been unclear due to the lack of suitable genetic tools and molecular analyses. In the present study, we established a novel zebrafish transgenic line with a promoter of *charon*, in which all KV-epithelial cells and their descendants are specifically labelled until the larval stage. We found that KV-epithelial cells underwent epithelial-mesenchymal transition upon KV-collapse and infiltrate into adjacent mesodermal progenitors, the presomitic mesoderm and chordoneural hinge. Once incorporated, the descendants of KV-epithelial cells expressed distinct mesodermal differentiation markers and contributed to the mature populations such as the axial muscles and notochordal sheath through normal developmental process. These results indicate that fully differentiated KV-epithelial cells possess unique plasticity in that they are reemployed into mesodermal lineages through transdifferentiation after they complete

their initial role in KV. (194 words)

Keywords (4-6 words)

charon, zebrafish, Kupffer's vesicle, transdifferentiation

Introduction

Kupffer's vesicle (KV) is a teleost-specific organ, which is transiently formed on the ventral side of the embryonic tailbud (Brummett and Dumont, 1978; Kupffer, 1868). KV consists of a fluid-filled lumen and its surrounding epithelial cells (hereafter referred to as KV-epithelial cells), and functions as the left-right organizer (LRO), playing a crucial role in left-right axis formation in the embryo (Essner et al., 2005). In the zebrafish, KV-epithelial cells are derived from a special group of cells called dorsal forerunner cells (DFCs; Melby et al., 1996; Oteíza et al., 2008). DFCs originally bear endodermal character as they express endoderm-specific genes, *sox32* and *sox17* (Alexander et al., 1999; Kikuchi et al., 2001; Warga and Kane, 2018). During epiboly stages, DFCs are transformed into KV-epithelial cells through mesenchymal-epithelial transition (Amack et al., 2007; Matsui et al., 2015; Oteíza et al., 2008; Zhang et al., 2016). At early somite stages, each KV-epithelial cell protrudes a primary cilium on the apical side, which rotates and generates the leftward fluid flow in the KV lumen (Essner et al., 2005). Sensed by primary cilia themselves, the leftward flow induces left-right asymmetric gene expression in and around KV, leading to left-sided expression of *nodal* in the lateral plate mesoderm (LPM; Essner et al., 2005). Judged by their morphological characteristics and specialized function, KV-epithelial cells are considered as fully

differentiated and functional cells.

In the light of the fate plasticity in matured cells, we were interested in the fate of KV-epithelial cells after they complete their mission in left-right patterning. Indeed, KV collapses and disappears soon after the establishment of the asymmetric gene expression in the LPM (hereafter referred to as KV-collapse), but previous lineage-tracing studies of DFCs demonstrated that upon KV-collapse, descendants of DFCs are incorporated into mesodermal tissues such as notochord, somites and tail mesenchyme (Cooper and D'Amico, 1996; Melby et al., 1996). However, detailed tracking and molecular characterization of those incorporated cells have not been performed so far, and thus we do not know yet whether ciliated KV-epithelial cells actually possess fate plasticity to transdifferentiate into functional mesodermal cells.

Recently, several transgenic zebrafish lines that express fluorescent proteins in DFCs and KV were generated for easier and more reliable tracing of DFC- and KV-derived cells. Among them, *sox17* lines have been frequently used because *sox17* promoter uniformly labels both DFCs and KV-epithelial cells from epiboly to somitogenesis stages (Compagnon et al., 2014; Mizoguchi et al., 2008; Oteíza et al., 2008; Sakaguchi et al., 2006). Furthermore, a recent work using *sox17:GFP-CAAX* line reported the epithelial-to-mesenchymal transition (EMT) of KV-epithelial cells during

KV-collapse (Amack, 2021), but their fate after EMT has not been directly tracked yet. For specific fate tracking of KV-epithelial cells, the *sox17* lines are not necessarily suitable, because endodermal cells as well as DFCs are broadly labelled (Mizoguchi et al., 2008). Other transgenic lines marking KV-epithelial cells (summarized in Table 1) have a similar limitation (Caron et al., 2012; Chen et al., 2012; Du and Dienhart, 2001; Molina et al., 2007). Thus, for precise tracing, another transgenic line was required in which mature KV-epithelial cells are specifically and uniformly labelled.

Here, we established novel transgenic lines, in which entire KV-epithelial cells are specifically labelled, using the promoter of *charon*. *charon* encodes a secreted Nodal antagonist belonging to the DAN family (Hashimoto et al., 2004). Its expression starts shortly after the differentiation of KV-epithelial cells from DFCs, and is highly specific to KV-epithelial cells both in zebrafish and medaka (Hashimoto et al., 2004; Hojo et al., 2007). The expression of *charon* is initially symmetric, but gradually becomes right-sided under the control of the leftward flow in KV (Hojo et al., 2007; Lopes et al., 2010). The essential role of *charon* in the left-right pattering is conserved among vertebrates as *charon*-knockout mice and zebrafish both exhibit randomized left-right axis (Marques et al., 2004; Montague et al., 2018).

Using these *charon* lines, we first confirmed that after KV-collapse, KV-derived

cells (KVDCs) differentiate into mesodermal but not into ectodermal or endodermal tissues. Detailed timelapse imaging and gene-expression analyses further revealed that KVDCs undergo EMT and infiltrate into two types of undifferentiated mesoderm, which are the presomitic mesoderm and the chordoneural hinge. Importantly, they expressed differentiation markers similar to their surrounding mesodermal cells at later stages. These findings demonstrate that KV-epithelial cells possess high plasticity after completing their initial role in KV, and that they transdifferentiate into mesodermal lineages during normal development.

Table 1: Transgenic lines in zebrafish for the visualization of DFCs and KV-epithelial cells

Promoter	Expression area at epiboly and somite stage	Timing	Length	Literature
crestin	Dorsal enveloping layer and KV	From DFCs (~50% epiboly)	1 kb	Chen et al., 2012
foxj1	Pronephric duct, floor plate and KV	From DFCs (~95% epiboly)	0.6 kb	Caron et al., 2012
dusp6	Mid-hindbrain boundary, Rhombomere 4and KV	From DFCs (bud stage)	10 kb	Molina et al., 2007
sox17	Endoderm and KV	From DFCs (~80% epiboly)	5.0 kb	Sakaguchi et al., 2006; Oteíza et al., 2008
twhh	Notochord and KV	From 12 hpf	5.2 kb	Du & Dienhart, 2001
charon	KV	From ~6 somite stage	5.0 kb	Gourronc et al., 2007; the present study

Results

Establishment of *charon:EGFP* to specifically label KV-epithelial cells

To establish transgenic lines in which KV-epithelial cells are specifically labelled, we cloned the 5-kb upstream sequence of zebrafish *charon* (Fig.1a, Supplementary Fig.1). A previous transient promoter assay demonstrated that the upstream sequence of zebrafish *charon* drives the reporter expression around KV (Gourronc et al., 2007), but any stable transgenic line using the *charon* promoter has yet to be established. After confirming the previous report by the Tol2-mediated EGFP reporter assay (Supplementary Fig.3a), we established three stable transgenic lines in which either EGFP, Lck-mGreenLantern (mGL) or H2B-mEosEM (a nuclear-localizing form of a photoconvertible fluorescent protein mEosEM; Fu et al., 2020) expression is driven by the *charon* 5-kb promoter (Fig.1b, Supplementary Fig.4a). In all the lines established, reporter gene expression was specifically detected in KV-epithelial cells (Fig.1c-e, Supplementary Fig.4b, c). In *charon:EGFP* embryos, EGFP fluorescence started to be detected from around the 6-somite stage (ss) just like endogenous *charon* (Hashimoto et al., 2004), and became stronger as KV grows in size. DAB (3,3'-Diaminobenzidine, tetrahydrochloride) immunohistochemistry against EGFP showed that at 6 ss and 12 ss, EGFP expression is strictly limited to the entire KV-epithelial cells with no ectopic

122 expression in adjacent mesoderm (Fig.1d-f). Fluorescence *in situ* hybridization with
123 immunofluorescence (FISH-IF; He et al., 2020) of *charon* in *charon:EGFP* embryos
124 further showed that *charon* expression mostly overlaps with that of EGFP at 12 ss
125 (Fig.1g). However, unlike endogenous *charon*, EGFP expression did not exhibited left-
126 right bias (Fig.1d-f). This can be explained by the fact that 3' untranslated sequence of
127 *dand5* (a mouse ortholog of *charon*) is responsible for its right-sided expression
128 (Minegishi et al., 2021; Nakamura et al., 2012). Untranslated sequences of zebrafish
129 *charon*, which are not included in the plasmid construct of this study, could have a
130 similar function to that of mouse *dand5*.

131 Furthermore, we found that the activity of upstream sequences of *charon* in KV-
132 epithelial cells is conserved among teleosts. A transgenic medaka (*Olyzias latipes*),
133 which was established with the upstream sequence of medaka *charon* (Supplementary
134 Fig.2), exhibited EGFP-reporter expression in KV-epithelial cells from 4 ss with faint
135 ectopic expression in the notochord (Supplementary Fig.5c). Overall, these results show
136 that *charon* transgenic lines are best suitable for the study of development and function
137 of KV-epithelial cells.

138

KVDCs differentiate into mesodermal lineages

KV is a transient organ and starts to degenerate at mid-somite stages (14–16 ss) when asymmetric *nodal* expression is established in the LPM (Cooper and D'Amico, 1996; Long, 2003; Supplementary Fig.8). However, we observed that EGFP-expressing cells in *charon:EGFP* embryos survived after KV-collapse and even persisted in hatched larvae (Supplementary Fig.3). Hereafter we refer to the EGFP-positive cells in *charon:EGFP* after KV-collapse as "KV-epithelium-derived cells (KVDCs)" to distinguish them from KV-epithelial cells. To track KVDCs after KV-collapse, we histologically analyzed embryos at the mid-somite stage (22 ss) and larvae at 3 days post fertilization (dpf) using DAB immunohistochemistry and confocal microscopy. In 22-ss embryos whose KVs have already diminished, most KVDCs were clustered around the collapsed lumen, but some of them were found in the adjacent notochord and presomitic mesoderm (PSM; Fig.2a, b). In 3-dpf hatched larvae, KVDCs were broadly distributed in the region posterior to the cloaca where no endodermal tissue exists (Fig.2c). KVDCs were detected in mesodermal tissues including both segmented and unsegmented posterior-most somites (Moriyama et al., 2012; Fig.2c, e1, e2), notochord cells near the posterior end and the notochordal sheath in the more anterior side (Fig.2d, e3), and fin mesenchymal cells with radial filopodia especially in the caudal fin fold

(Fig.2c, d and e4). We counted the number of KVDCs in each tissues using *charon:H2B-mEosEM* 3-dpf larvae and found that they were most abundant in the unsegmented posterior-most somites (56±11 cells/embryo; Fig.2f). In contrast, no KVDCs were observed in the ectoderm (Fig.2d, e).

To further support the above findings, we directly examined the migration of KVDCs into these mesodermal tissues by a photoconversion-based method (Shimada et al., 2013). We photoconverted H2B-mEosEM transiently expressed in KV-epithelial cells of *βactin:memCherry* embryos, whose cell membrane is labelled with mCherry (Xiong et al., 2014). After photoconversion at around 13 ss, labelled KV-epithelial cells were tracked at an interval of 1 hour during segmentation periods (n = 4 embryos, Fig.2g). At 14 ss (0 hour after photobleaching), photoconverted H2B-mEosEM was only detected in KV-epithelial cells, confirming the specificity of photoconverted labelling (Fig.2h). The labelled KVDCs tended to stay together until 19 ss (4 hours after photobleaching), and then gradually migrated from KV into the PSM and notochord (Fig.2h, arrowheads in the 28-ss panel). When the same embryos were further observed at 2 dpf, the labelled KVDCs were broadly distributed in segmented somites, unsegmented posterior-most somites, and the notochord (Fig.2h, arrowheads in the 2-dpf panel). We obtained a similar result using another transgenic line, *foxj1a:KikGR*, in

which photoconvertible protein KikGR (Tsutsui et al., 2005) is expressed in KV-epithelial cells as well as in the floor plate (Caron et al., 2012; Supplementary Fig.7a). Taken together, the results demonstrated that KVDCs migrate and contribute to the axial and paraxial mesoderm.

Loss of the LRO and epithelial character in KVDCs

We next examined the molecular characteristics of KVDCs after KV-collapse. We first examined whether any KVDCs are eliminated by apoptosis during and after KV-collapse. Immunostaining of cleaved caspase-3, an executioner of apoptotic process (Elmore, 2007), revealed that apoptosis was induced in KVDCs after KV-collapse, but that the number of apoptotic KVDCs was limited (Fig.3a, b). We then asked how survived KVDCs lost morphological and molecular characteristics of the LRO components by examining *charon* (LRO marker) and *sox17* (DFCs marker) expression and the protein distribution of ZO-1 (epithelial marker) and acetylated α-tubulin (primary cilia marker) in KVDCs (Alexander and Stainier, 1999; Essner et al., 2005; Hashimoto et al., 2004; Oteíza et al., 2008). FISH-IF showed that the expression of *charon* was diminished at 20 ss and 26 ss compared to at 12 ss, and *charon*-negative KVDCs were frequently detected (Fig.3c). Moreover, we did not detect *sox17*

193 expression in KV-epithelial cells or KVDCS at all stages examined (Supplementary
194 Fig.6), which is consistent with the previous report (Alexander and Stainier, 1999).
195 ZO-1 was accumulated on the surface of the KV lumen at 6 ss, confirming the
196 epithelial character of EGFP-positive cells in *charon:EGFP* (Fig.3d; Oteíza et al., 2008).
197 At 18 ss, shortly after KV-collapse, migrating KVDCs no longer expressed ZO-1,
198 although residual ZO-1 expression was detected in a cluster of KVDCs located on the
199 ventral side of the CNH. At 26 ss, a substantial number of KVDCs moved to the
200 posterior edge of the chordoneural hinge (CNH), a group of progenitors which are
201 located at the posterior end of the notochord and thought to give rise to the notochord,
202 floor plate and hypochord (Agathon et al., 2003; Row et al., 2015). Furthermore,
203 primary cilia of KVDCs were largely diminished after KV-collapse, particularly in
204 migrating ones (Fig.3e). Taken together, the results suggest that KV-epithelial cells
205 gradually lose their LRO and epithelial character, and acquire mesodermal fates through
206 mid-to late somite stages.
207
208 KVDCs undergo EMT at the onset of migration
209 We examined detailed cellular behavior of KVDCs at the onset of migration using a
210 double transgenic line, *charon:EGFP;βactin:memCherry*. KV initially protruded into

the yolk, then incorporated into the tailbud at around 10 ss, and finally collapsed (Supplementary Figure 8). At around 14 ss, KV-epithelial cells detached from the underlying yolk syncytial layer (YSL) (Fig.4, Supplementary Video 1). Interestingly, a ring-like structure labelled by strong mCherry signals appeared in the YSL just beneath KV (Fig. 4, magenta arrowheads). This YSL ring shrank when KV was detached from the YSL as if it pushes KV out into the tailbud and breaks the connection between KV and the YSL. Once KV was detached from the YSL, its lumen started to shrink (Fig. 4, the 01:20 panel). At the same time, KV-epithelial cells started to disperse and migrate, extending filopodia-like structures (Fig. 4, insets in the 02:40 panel, Supplementary Video 2). This observation, together with the loss of ZO-1 expression (Fig.3d), suggests that KV-epithelial cells undergo epithelial-mesenchymal transition during KV-collapse.

Differentiation of KVDCs into the PSM and somite derivatives

We next examined the developmental capacity of KVDCs which migrate into somites using lineage-specific differentiation markers. At 12 ss when KV is still present, KV epithelial cells were ventrally attached to the PSM as well as notochord (Fig.5a). A pan-PSM marker *msgn1* (Joseph and Cassetta, 1999; Yoo et al., 2003; Yoon et al., 2000) was strongly expressed in the PSM but not in KV-epithelial cells at 12 ss (Fig.5a),

confirming their distinct lineages. After KV-collapse, KVDCs were found in the PSM (Fig.5b1) and later in the anterior segmented somites as well, where *msgn1* expression is no longer detected (Fig.5b2). These results suggest that KVDCs are incorporated into the PSM after KV-collapse and are intermingled with surrounding PSM cells.

The zebrafish somite consists of three populations with distinct fates, the myotome, dermomyotome, and sclerotome (Stickney et al., 2000). The myotome is further divided into the two subpopulations, slow muscle in the dorsal (outer), and fast muscle in the ventral (deeper) regions. KVDCs were found to be distributed in all these populations at later stages (Fig.5). At 3 dpf, KVDCs which are located near the surface and in the deep layer of the myotome expressed slow and fast muscle markers, respectively, as detected by F59 and F310 antibodies (Fig.5c, d). These muscle cells persisted at least until 5 dpf (data not shown), suggesting that they differentiated into functional muscles. Fast muscles are known to be derived from adaxial cells which are large, cuboidal in shape, located adjacent to the notochord and express *myoD* (Devoto et al., 1996). During slow muscle development, adaxial cells radially migrate from their original position toward the superficial layer of the myotome and differentiate into slow muscles there (Barresi et al., 2001; Cortés et al., 2003). At late somite stage (26 ss), we identified adaxial cell-like KVDCs, judged by their shape and location, and found that

they indeed expressed *myoD* (Fig.5h). This observation suggests that KVDCs follow the normal developmental process to differentiate into slow muscles.

KVDCs were also found in the dermomyotome layer (the outer-most surface of the somite) and in the sclerotome region (the ventro-medial region near the notochord and neural tube), where they expressed the dermomyotome marker, Pax3/7 (Hammond et al., 2007) and sclerotome marker, *nkx3.1* (Ma et al., 2018), respectively (Fig.5e, i). We also examined the positional relationship between ventral KVDCs and posterior blood vessels, because the ventral sclerotome is known to differentiate into mural cells, which surround blood vessels (Stratman et al., 2017). For this, we used double transgenic fish of *charon:EGFP* and *drl:mCherry*, whose LPM derivates are specifically labelled with mCherry (Mosimann et al., 2015; Prummel et al., 2019). We found that phalloidin-negative KVDCs were attached to the posterior-most part of the caudal vein (Fig.5f, g), supporting the idea that KVDCs acquire the differentiation potency of the sclerotome. Importantly, KVDCs did not overlap with mCherry-expressing LPM-derivatives, indicating that they do not contribute to the LPM lineage (Fig.5f, g).

Differentiation of KVDCs into the notochord and tail mesenchyme

We further examined the differentiation process of KVDCs in the notochord and tail

mesenchyme. At 12 ss, KV-epithelial cells were ventrally attached to the *no tail* (*ntl*, the young notochord marker)-positive notochord (Schulte-Merker et al., 1994; Fig.6a). At 20 ss, some KVDCs were found in the posterior end of *ntl*-expressing area, i.e., the CNH (Fig.6b). These KVDCs were also positive for *ntl*, indicating that they had acquired the axial mesodermal fate. Some KVDCs further developed into *ntl*-negative mature notochord cells at 26 ss (Fig.6b), and later into the surrounding sheath cells (Fig.2d). These results show that KVDCs which infiltrate into the CNH possess the full capacity of notochord differentiation.

The migration of KVDCs into the axial mesoderm seemed to take place exclusively in the CNH. The developing and mature notochord is surrounded by the basement membrane formed by deposition of extracellular matrix (ECM) such as Laminin and Fibronectin (Scott and Stemple, 2004). However, accumulation of these two major ECM components was reduced around the CNH as indicated by immunostaining (Fig.6d, e), which may facilitate cell mingling and infiltration of KVDCs into the CNH.

Lastly, we tracked the fate of the posterior-most KVDCs cluster which stays around the CNH until the end of the segmentation period (Fig.3d). We found that these KVDCs are distinguished from CNH cells, because they did not express the CNH

283 markers, *noto* and (Dheen et al., 1999; Fig.6c). Using *charon:H2B-mEosEM*, we
284 examined the fate of these KVDCs by photoconverting H2B-mEosEM-expressing cells
285 located posterior to the CNH at around 28 ss and chased the labelled cells in 2 dpf
286 larvae. The result demonstrated that they preferentially differentiated into fin
287 mesenchymal cells in the caudal fin fold rather than into the CNH or notochord cells (n
288 = 3 embryos, Fig.6f). These results imply that these KVDCs occupy a posterior-most
289 part of the paraxial (but not the axial) mesoderm and directly differentiate into caudal
290 fin mesenchyme.
291

Discussion

During differentiation, the potency of cells becomes restricted as they are specified into certain lineages. In some contexts, however, differentiated cells can be converted to other cell types; a phenomenon called adult cell plasticity (Merrell and Stanger, 2016). Such plasticity is often observed in the regeneration process, but it is still a matter of debate whether it takes place commonly during normal development of animals (Merrell and Stanger, 2016). The present study demonstrated that derivatives of KV-epithelial cells (KVDCs) join mesodermal progenitors after KV-collapse and differentiate into mature cell types according to their location. Such “reemployment” of KV-epithelial cells is a rare example of cell plasticity of fully differentiated cells during normal development in vertebrates, which is achieved through transdifferentiation (Fig.7).

KVDCs are a multipotent mesodermal cell population in the tailbud

Our results revealed that KVDCs in the zebrafish tailbud possess unique differentiation potency. The zebrafish tailbud contains three undifferentiated cell populations, the PSM, CNH, and neuromesodermal progenitors (NMPs; Beck, 2015; Sambasivan and Steventon, 2021). KVDCs occupy a part of the PSM and CNH, and differentiate into the paraxial and axial mesoderm. In contrast, KVDCs never contribute to NMPs as they do

not give rise to the neural tube (Henrique et al., 2015). Importantly, KVDCs are unique among these progenitors in the tailbud in that they are the descendants of functional epithelial cells with primary cilia, which exerted a crucial role in left-right patterning.

The contribution of the LRO cells to the mesodermal tissues could be a common feature among vertebrates, although the origin and structures of the LRO are diverse (Blum et al., 2014). The gastrocoel roof plate in amphibians and node in mammals, which function as the LRO in these species (Blum et al., 2014), are suggested to differentiate into the notochord and somites, and into the posterior notochord, respectively (Brennan et al., 2002; Shook et al., 2004). Thus, it is likely that the vertebrate LRO cells generally behave as mesodermal cells at later stages, although DFCs in the zebrafish are transiently endodermal at the beginning of their emergence (Alexander and Stainier, 1999).

Transdifferentiation of KVDCs

Transdifferentiation of mature cells is generally achieved through dedifferentiation into a potent state followed by redifferentiation into a new lineage (Jopling et al., 2011). The development of KVDCs appears to go through this process: KVDCs redifferentiate into somite-derivatives and notochord after being integrated into their progenitors. We observed that KV-epithelial cells undergo EMT during KV-collapse. EMT frequently

330 occurs in association with dedifferentiation as seen in cancer metastasis and neural crest
331 delamination (Yang and Weinberg, 2008). Indeed, EMT in KV is accompanied by the
332 loss of differentiated epithelial characters such as primary cilia and tight junctions,
333 which lead to KV-collapse and cell migration. Factors triggering this EMT are yet to be
334 determined, although potent signalling ligands, Wnt, BMP and FGF are produced in the
335 nearby PSM (Hubaud and Pourquié, 2014; Row and Kimelman, 2009). Furthermore, we
336 described the shrinkage of the YSL underlying KV in the present study (Fig.4c). This
337 shrinkage might generate mechanical force which triggers EMT in cooperation with
338 those signalling ligands (Gjorevski et al., 2012).

339 In general, mature epithelial cells maintain their fate and integrity by cell-cell
340 junctions and attachment to the basement membrane (Yang et al., 2020). Then, why can
341 KV-epithelial cells undergo transdifferentiation and what makes them so unique?
342 Despite the presence of evident apico-basal polarity and cell-cell junctions, KV
343 epithelium seems to lack the basement membrane, as revealed by our immunostaining
344 and a previous report on the atypical localization of Laminin β1a to their apical side
345 (Hochgreb-Hägele et al., 2013). Thus, KV-epithelial cells may not be of typical
346 epithelium in character, which could reflect their transient function. Lack of the
347 basement membrane would allow KV-epithelial cells to dedifferentiate and migrate

without a need of ECM remodelling.

Some vertebrate tissues consist of cells derived from different lineages. The prominent examples are the zebrafish pituitary and mammalian vascular endothelium, where undifferentiated cells from different origins converge at the transcription level once they are intermingled (Fabian et al., 2020; Plein et al., 2018). We confirmed here that KVDCs, whose origin is distinct from the authentic mesoderm, differentiate into the notochord and somite-derivatives in the caudal region. KVDCs are thus a good model for the study of such lineage convergence during normal development. Single-cell multiomics using *charon* transgenic lines will provide insights into the mechanism of how and to what extent cells from different lineages converge together to form a functionally integrated tissue.

Figure legends

Figure 1. Establishment of *charon:EGFP* for the specific labeling of KV-epithelial cells

a, Location of the 5-kb *charon* promoter in the zebrafish genome. *charon* resides on chromosome 1, and the 5-kb *charon* promoter spans from the direct upstream position of its start codon.

b, Construction of *charon:EGFP* transgene flanked by Tol2 excision sites.

c, Lateral view of the EGFP fluorescence in a *charon:EGFP* embryo at 9 somite stage (ss). Fluorescence image was merged with the DIC (differential interference contrast) image. KV, Kupffer's vesicle.

d, Dorsal view of a *charon:Lck-mGL* embryo at 9 ss injected with H2B-mCherry mRNA. Black arrowhead indicates the level of the sagittal optical section on the right side.

e, Dorsal view of a DAB-stained *charon:EGFP* embryo at 12 ss.

f, Cross section of the tailbud of a DAB-stained *charon:EGFP* embryo at 12 ss. Nuclei were counterstained with hematoxylin. Dorsal side to the top.

g, FISH-IF of *charon* in a *charon:EGFP* embryo at 12 ss. Magenta signal is for FISH of *charon* mRNA whereas green is for immunostaining of EGFP proteins. Lateral view of

the tailbud region is shown. White box indicates the enlarged area. Dorsal to the bottom, posterior to the left. Scale bars, 200 µm (c, e), 100 µm (f) and 50 µm (d, h).

Figure 2. Histology of KVDCs

a, Lateral view of a DAB-stained *charon:EGFP* embryo at 22 ss. White arrowheads indicate KVDCs which have started to migrate.

b, Cross section of the tailbud of a DAB-stained *charon:EGFP* embryo at 22 ss. Nuclei were counterstained with hematoxylin. Dorsal side to the top. PSM, presomitic mesoderm. nc, notochord.

c, Lateral view of a *charon:EGFP* embryo at 22 ss counterstained with phalloidin and DAPI. Dorsal to the top. Green arrowheads indicate EGFP-positive cells in the CNH (chordoneural hinge).

d, Cross sections of a DAB-stained *charon:EGFP* larva at 3 dpf. Nuclei were counterstained with hematoxylin. Dorsal side to the top. Asterisk indicates a melanocyte. dmu, dorsal muscle. fm, fin mesenchyme. nc, notochord. ncs, notochordal sheath. nt, neural tube. vmc, ventral muscle.

e, Lateral view of the caudal region of a *charon:EGFP* embryo at 3 dpf counterstained with phalloidin. White boxes indicate areas magnified in the panels 1-4. White dashed

line indicates the edge of the fin fold. Panel 1, EGFP-positive muscles in segmented somites. Panel 2, EGFP-positive muscles in non-segmented somites. Panel 3, EGFP-positive notochord cells. Panel 4, EGFP-positive fin mesenchymal cells in the caudal fin fold. Scale bars, 200 μm (a, e), 100 μm (b, d), 50 μm (c).

f, Number of H2B-mEosEM-positive KVDCs in *charon:H2B-mEosEM* in four populations shown in (e). Horizontal bars, mean. Vertical bars, standard deviation. N = 20 larvae.

g, Scheme for the labelling of KV-epithelial cells by photoconversion. H2B-mEosEM is expressed in KV-epithelial cells in *βactin:memCherry* embryos by injection of *charon:H2B-mEosEM* plasmid. H2B-mEosEM was photoconverted at around 13 ss using a confocal microscopy and time-lapse images were taken every 1 hour.

h, Time-lapse images of a *βactin:memCherry* embryo injected with *charon:H2B-mEosEM*. Images taken every 2 hours after photoconversion and from 2 dpf treated larvae are shown. Arrowheads indicate the migrated KVDCs labelled with photoconverted H2B-mEosEM.

Figure 3. Loss of the LRO character in KVDCs

a, Immunostaining of cleaved caspase-3 in *charon:EGFP* embryos at 12, 20 and 26 ss.

Top, the signal of cleaved caspase-3. Bottom, merged view with EGFP and DAPI signal. Magenta arrowheads indicate KVDCs which is positive for cleaved caspase-3.

b, Quantification of cleaved caspase-3-positive KVDCs. Horizontal bars, mean. Vertical bars, standard deviation. *p*-values from two-tailed Welch's t-test are shown. N = 9 (12 ss), 11 (20 ss), and 10 (26 ss) embryos.

c, FISH-IF of *charon* in *charon:EGFP* at 20 and 26 ss. Magenta, signal of FISH for *charon* mRNA. Green, signal of immunostaining for EGFP. Lateral view of the tailbud region is shown. Dorsal to the top.

d, Immunostaining of ZO-1 in *charon:EGFP*. KV is shown for 6 ss whereas the tail region is shown for 18 and 26 ss. Magenta and white arrowheads indicate KVDCs with and without ZO-1 expression, respectively. nc, notochord. CNH, chordoneural hinge.

e, Immunostaining of acetylated α-tubulin in *charon:EGFP*. Magenta and white arrowheads indicate KVDCs with and without acetylated α-tubulin signal, respectively. Scale bars, 50 μm (a, c, d, e).

Figure 4. KVDCs migrate to mesodermal tissues through EMT

Time-lapse images of a *charon:EGFP;βactin:memCherry* embryo taken every 20 minutes for 3 hours from 13 ss. Magenta arrowheads indicate the shrinkage of the YSL

underlying KV. White boxes in the panel 02:40 indicate inset areas. Green arrowhead in the inset indicates a filopodium-like structure formed in KVDCs. Scale bars, 50 μm.

Figure 5. Differentiation of KVDCs into somite derivatives

a, FISH-IF of *msgn1* in a *charon:EGFP* embryo at 12 ss. Left, dorsal view. Top, an optical section at the level of the dashed line in the panel below. Right, a more dorsal stack than the left one. PSM, presomitic mesoderm.

b, FISH-IF of *msgn1* in *charon:EGFP* embryos at 20 ss and 26 ss. Left, dorsal view. Anterior to the top. Right, optical sections at the level of the dashed lines in the left panels. White arrowheads indicate KVDCs in the PSM (20 ss and 26 ss) and in the segmented somites (26 ss).

c, d, Vibratome cross sections of *charon:EGFP* 3 dpf larvae immunostained with F59 (c) and F310 (d) antibodies to show the distribution of slow and fast muscles, respectively. Counterstaining was performed with DAPI. White arrowheads indicate EGFP-positive slow and fast muscle cells. Dorsal to the top. nt, neural tube. nc, notochord.

e, Immunostaining of dermomyotomes by anti-Pax3/7 antibody in a *charon:EGFP* 2 dpf larva. Lateral view and optical sections at the level of dashed lines are shown. White

arrowheads indicate EGFP-positive dermomyotomes.

f, Lateral view of a *charon:EGFP;drl:mCherry* 3 dpf larva. White arrowheads indicate EGFP-positive sclerotomal cells surrounding mCherry-positive cells derived from the LPM. nc, notochord. LPM, lateral plate mesoderm.

g, Left, cross section of a *charon:EGFP;drl:mCherry* 3 dpf larva immunostained with anti-EGFP and anti-mCherry antibodies. Counterstaining was performed with phalloidin and DAPI. Right, a magnified view of the white rectangular area in the left panel. White arrowheads indicate KVDCs surrounding mCherry-positive LPM derivatives.

h, i, FISH-IF of *myod1* in a *charon:EGFP* embryo at 26 ss (h) and *nkx3.1* in a 24 hpf (hours post fertilization) embryo (i). Left panel, lateral view. Anterior to the left, dorsal to the top. Right panel, optical sections at the level of the dashed lines in the left panels. White arrowheads indicate KVDCs which differentiated in *myod1*-positive adaxial cells (h) and *nkx3.1*-positive sclerotomes (i). Scale bars, 50 μm (a-i).

Figure 6. Differentiation of KVDCs into the notochord

a, FISH-IF of *ntl* in a *charon:EGFP* embryo at 12 ss. Top, dorsal view. Anterior to the top. Bottom, an optical section at the level of the dashed line in the upper panel. nc, notochord.

b, FISH-IF of *ntl* in *charon:EGFP* embryos at 20 ss and 26 ss. Dorsal views. Anterior to the left. White arrowheads, KVDCs in the CNH (20 ss) and in the notochord (26 ss). CNH, chordoneural hinge.

c, d, Immunostaining of Laminin (c) and Fibronectin (d) in *charon:EGFP* embryos at 12 ss and 20 ss. For 12 ss, dorsal views of KV are shown. Anterior to the top. For 20ss, lateral views of the tailbud are shown. Dorsal to the top. Anterior to the right.

e, FISH-IF of *noto (flh)* in a *charon:EGFP* embryo at 26 ss. Lateral view. Dorsal to the top. Anterior to the left.

f, Lineage tracing of the KVDCs cluster at the posterior tip of the CNH. H2B-mEosEM was expressed in KVDCs by *charon:mEosEM* plasmid injection into *βactin:memCherry* embryos. Photoconversion was performed in 28 ss and the labelled KVDCs were chased at 2 dpf. White arrowheads indicate the labelled KVDCs which differentiated into fin mesenchymal cells in the caudal fin fold. Scale bars, 50 μm (a-f).

Figure 7. An overview of KVDCs differentiation

Schematic diagram depicting the process of the transdifferentiation-mediated reemployment of KV-epithelial cells. After KV-collapse, KV-epithelial cells dedifferentiate and undergo EMT. Mesenchymalized KVDCs infiltrate into mesodermal

progenitors, the PSM and CNH, and acquire new fates according to their new locations. Note that they do not directly migrate to the segmented somites or the mature notochord.

Supplementary Figure 1. Sequence of the zebrafish 5-kb *charon* promoter

Nucleotide sequence of the 5-kb *charon* promoter in the zebrafish.

Supplementary Figure 2. Sequence of the medaka 5-kb *charon* promoter

Nucleotide sequence of the 5-kb *charon* promoter in medaka. Red, partial coding sequences of *charon* gene.

Supplementary Figure 3. Fluorescence stereomicroscope images of *charon:EGFP*

a, Lateral view of a *charon:EGFP* embryo at 6 ss.

b, Ventral view of a *charon:EGFP* embryo at 20 ss .

c, Lateral view of a *charon:EGFP* larva at 2 dpf. Scale bars, 200 μm (a-c).

Supplementary Figure 4. Fluorescence of *charon:Lck-mGreenLantern*

a, The construction of *charon:Lck-mGreenLantern* transgene.

b, c, Lateral view of a *charon:Lck-mGreenLantern* embryo at 8 ss (b) and 22 ss (c). KV, Kupffer's vesicle. Scale bars, 200 µm.

Supplementary Figure 5. Medaka *charon* promoter is active in medaka KV-epithelial cells

a, Location of the *charon* 5-kb promoter in the medaka genome. *charon* resides on chromosome 1, and the *charon* 5-kb promoter spans from the direct upstream position of its start codon.

b, Construction of *Ol_charon:EGFP* transgene flanked by I-SceI recognition sites.

c, Expression of EGFP in *Ol_charon:EGFP* embryos. Lateral views on the top row, dorsal views on the bottom row. White dot lines indicate embryonic bodies. Red circle indicates the position of KV. Scale bars, 500 µm.

Supplementary Figure 6. FISH-IF of *sox17* in *charon:EGFP* embryos

FISH-IF of *sox17* in *charon:EGFP* embryos at 6 ss, 12 ss, 20 ss and 26 ss. Lateral views of tailbud regions are shown. Scale bars, 50 µm.

Supplementary Figure 7. *foxj1a:KikGR* supports KV-epithelial cell migration

a, Scheme for the photoconversion labelling of KV-epithelial cells in *foxj1a:KikGR*. KikGR in KV-epithelial cells was selectively photoconverted at around 13 ss and time-lapse images were taken every 1 hour.

b, Time-lapse images of a photoconverted *foxj1a:KikGR* embryo. Single stacks from images taken every 2 hours after photoconversion are shown. When photoconverted at around 13 ss, labelled KVDCs migrated into the PSM and the notochord by 28 ss (6 hours after photoconversion). Scale bars, 50 μm.

Supplementary Figure 8. Time-lapse imaging of the incorporation of KV into the tailbud

Time-lapse imaging of the KV development in a TL2E embryo. Arrowheads indicate the position of KV. Staring from 4 ss, images are taken every 15 minutes for 10 hours. Scale bars, 50 μm.

Supplementary Video 1. Time-lapse imaging of KV-collapse

A video showing the process of KV-collapse in a *charon:EGFP;βactin:memCherry* embryo. Time-lapse images were taken every 5 minutes for 3 hours from 13 ss. Note

539 that a ring-like structure is formed beneath KV during KV-collapse. Scale bar, 50 μm.

540

541 Supplementary Video 2. Formation of filopodia-like structures in KVDCs

542 Green channel is extracted from Supplementary Video 1 to show the formation of

543 filopodia-like structure in KVDCs. Scale bar, 50 μm.

544

Author Contributions

Conceptualization, T.I., K.I., and H.T.; Methodology, T.I., K.I., and T.K.; Investigation, T.I., K.I., and T.K.; Resources, T.I., K.I., and T.K.; Writing - Original Draft, T.I.; Writing - Review & Editing, T.I., T.K., and H.T.; Supervision, H.T.; Funding Acquisition, T.I., K.I., T.K. and H.T..

552 **Acknowledgement**

553 We thank S. Megason for *βactin:memCherry* strain; C. Mosimann for *drl:mCherry*

554 strain and *drl:EGFP (pCM298)* plasmid; N. H. Patel for Pax3/7 antibody (DP312); A.

555 Shimada for technical support and discussion; Y. Yamagishi, S. Tayama, I. Fukuda, M.

556 Funato and M. Sakamoto for fish husbandry. This work was supported by Grant-in-Aid

557 for Japan Society for the Promotion of Science (JSPS) Fellows under Grant Numbers

558 18J21960 (T.I.) and 15J08599 (K.I.), JSPS KAKENHI under Grant Numbers

559 JP19K23741 and JP21K15101 (T.K.) and Japan Agency for Medical Research and

560 Development (AMED) under Grant Number JP21gm1110007 (H.T.).

561

562

Competing interests

Materials & Correspondence

Material and Methods

Zebrafish strain and manipulation of embryos

The RW (RIKEN WT) and TL2E (Tüpfel long fin 2E) strains were used as the wild-type zebrafish strains. Adult fish and embryos were maintained under standard conditions. Fertilized embryos were incubated at 23-28°C in 1/3×Ringer's solution (38.7 mM NaCl, 0.97 mM KCl, 1.67 mM HEPES, 1.80 mM $CaCl_2$) to obtain the stage of interest. For imaging hatched larvae, 0.003% N-phenylthiourea (PTU) was added to 1/3×Ringer's solution during somitogenesis to prevent pigmentation. Staging of embryos is based on Kimmel et al. (1995). All experimental procedures and animal care were carried out according to the animal ethics committee of the University of Tokyo (Approval No. 20-2).

Plasmid construction

The sequences of *charon* and *foxj1a* promoters (5 kb and 5.2 kb, respectively) were amplified from the genomic DNA of the RW strain and were cloned into pCR Blunt II-TOPO vector (Invitrogen). pDestTol2pA2-*charon:EGFP* (*charon:EGFP* for short) was constructed by replacing the *drl* promoter in pDestTol2pA2-*drl:EGFP* (Mosimann et al., 2015) with the cloned *charon* promoter. Medaka *charon* promoter was cloned from

586 genomic DNA of medaka d-rR strain and was inserted into pBlueScript II SK(+)-EGFP
587 carrying an I-SceI cassette to make pBSSK-I-SceI-*Ol_charon:EGFP* (*Ol_charon:EGFP*
588 for short). pDestTol2pA2-*charon:Lck-mGreenLantern* was constructed as follows: the
589 CDS of mGreenLantern (Campbell et al., 2020) whose codon usage is optimized for
590 zebrafish was purchased from Integrated DNA Technologies (IDT), and was inserted
591 into pCSf107mT vector (Mii et al., 2009) with an N-terminal membrane localization
592 signal of mouse Lck (Chertkova et al., 2017) to make pCSf107-Lck-mGreenLantern.
593 Then, the CDS of Lck-mGreenLantern was subcloned into pDestTol2pA2 vector
594 carrying the *charon* promoter. pDestTol2pA2-*charon:H2B-mEosEM* was constructed as
595 follows: the CDS of mEosEM was synthesized through mutagenesis of mEos4b (Paez-
596 Segala et al., 2015) as described (Fu et al., 2020), and was assembled together with the
597 CDS of human Histone H2B type 1-J (H2BC11) into pCSf107mT to make pCSf107-
598 H2B-mEosEM. Then, the CDS of H2B-mEosEM was subcloned into pDestTol2pA2
599 vector carrying the *charon* promoter. To construct template plasmids for the antisense
600 probe synthesis, full-length coding sequences (CDSs) of zebrafish *charon*, *sox17*, *msgn1*,
601 *myod1*, *nkx3.1*, *ntl* and *noto* cloned from 16 ss cDNA were inserted into pCSf107mT.
602 These cloning and subcloning were performed using PrimeSTAR GXL polymerase,
603 PrimeSTAR MAX polymerase, In-fusion HD kit and In-Fusion Snap Assembly kit

(TaKaRa). pRSETa_mEos4b was a gift from Loren Looger (Addgene plasmid #51073; http://n2t.net/addgene:51073; RRID:Addgene_51073). Lck-mScarlet-I was a gift from Dorus Gadella (Addgene plasmid #98821; http://n2t.net/addgene:98821; RRID:Addgene_98821). Digital plasmid maps are available upon request.

Transgenesis

Zebrafish transgenesis was based on the Tol2 transposase method (Kikuta and Kawakami, 2009). To obtain founders, Tol2 mRNA (25 ng/µL) and plasmids (12.5 ng/µL) were injected into one-cell stage embryos of the RW strain. Founders carrying transgenes were screened by crossing with the TL2E strain. For medaka transgenesis, the I-SceI method (Rembold et al., 2006) was used. Following digestion with I-SceI, *Ol_charon:EGFP* plasmid was injected into one-cell stage embryos of the d-rR wildtype strain. Founders were screened by crossing with the d-rR strain. Fluorescence image of transgenic embryos was captured by M165 FC fluorescence stereomicroscope and DFC7000T digital camera (Leica).

Time-lapse imaging and photoconversion

To perform time-lapse imaging, embryos were mounted laterally in the chamber of 1%

agarose in 1/3×Ringer's solution with their left side down. Embryos were imaged by LSM710 confocal microscopy (Carl Zeiss) from 13 ss for 3 hours or longer at an interval of 5 min. In cell-tracking experiments, the photoconversion of H2B-mEosEM was performed with a 405 nm diode laser at the power of 10%. After photoconversion, embryos were released in 1/3x Ringer's solution with 0.003% PTU and were grown until they reach the stages of interest in a shaded chamber. The 3D rendering of time-lapse images was performed with Imaris (version 8.1.2, Bitplane).

Histology and immunostaining

Embryos were fixed with 4% paraformaldehyde (PFA) in PBST at 4°C overnight or at room temperature for 2 hours, washed with PBST for three times and were stored at 4°C until use (except for Laminin and Fibronectin, see below). Fixed embryos were permeabilized with 1% Triton X-100 in PBS, blocked with 2% BSA in PBSDT (PBS/1% DMSO/0.1% Triton X-100) and were immunostained with following antibodies: mouse monoclonal anti-GFP (1/100, A-11120, Invitrogen), rabbit poly-clonal anti-GFP (1/800, 632592, Clontech), anti-Myosin heavy chain (1/10, F59, deposited to the DSHB by Stockdale, F.E.), anti-Myosin light chain 1 slow and 3 fast (1/10, F310, deposited to the DSHB by Stockdale, F.E.), anti-Pax3/7 (1/500, DP312, by

courtesy of N. H. Patel), anti-DsRed (1/500, 632496, Clontech), anti-cleaved caspase-3 (1/500, 9661, Cell Signaling Technology), anti-phospho Histone H3 (1/500, 06-570, Merck), and anti-ZO-1 (1/50, 33-9100, Invitrogen). For immunostaining of Laminin and Fibronectin, embryos were fixed by 2% PFA for 2 hours at 25°C, then for overnight at 4°C. After quenching PFA with 50 mM glycine in PBSTT (PBS/0.5% Triton X-100/0.5% Tween 20) and subsequent washing, embryos were blocked with 5% BSA in PBSTT, and were stained with anti-Laminin (1/100, L9393, Sigma-Aldrich) or anti-Fibronectin (1/100, F3648, Sigma-Aldrich). Secondary antibodies for immunofluorescence were anti-rabbit IgG labelled with Alexa Fluor 488, 555, or 568 (A11008, A21429 or A10042, Invitrogen) and anti-mouse IgG labelled with Alexa Fluor 488 or 568 (A11001 or A10037, Invitrogen). For counterstaining, Phalloidin (labelled with Rhodamine or Alexa Fluor 647) (R415 or A22287, Invitrogen) and DAPI (4',6-diamidino-2-phenylindole) were added to the secondary antibody solution. Stained embryos were mounted with 1% LMP agarose/PBS (16520-050, Invitrogen) in a glass-based dish (3911-035, Iwaki) and were imaged by LSM710 confocal microscopy (Carl Zeiss). 40× and 25× water-immersion objective lenses (LD C-Apochromat 40x/1.1 W Korr M27 and LD LCI Plan-Apochromat 25x/0.8 Imm Corr DIC M27, Carl Zeiss) and a 5× objective lens (EC Plan-Neofluar 5x/0.16) were used. The contrast adjustment and

658 cropping of captured images were performed by Fiji (version 1.53c; Schindelin et al.,
659 2012).

660 For immunostaining of cross sections in 3 dpf larvae of *charon:EGFP*, fixed
661 specimens were embedded in 4% LMP agarose/PBS, and 100-200 μm sections were
662 prepared using Vibratome 3000 Tissue Sectioning System. Free-floating sections were
663 stained with appropriate antibodies and mounted with 50% Glycerol/PBS on a slide
664 glass.

665 For DAB staining of EGFP-expressing cells, fixed *charon:EGFP* embryos
666 were blocked with 0.3% H_2O_2 for 30 min and with 2% BSA in PBST for 2 hours,
667 stained with anti-GFP antibody (1/800, 632592, Clontech) and biotinylated anti-rabbit
668 IgG (1/200, BA-1000, Vector Laboratories). VECTASTAIN® Elite® ABC Kit (Vector
669 Laboratories) and DAB tablets (D5905, Sigma-Aldrich) were used for DAB
670 chromogenic reaction. Stained embryos were embedded in Technovit 7100 resin (Kulzer
671 Technique) and 5 μm sections were obtained using an RM2245 microtome (Leica).
672 Sections were counterstained with Mayer's hematoxylin solution and images were
673 captured by BX61 microscope (Olympus) and AxioCam MRc 5 camera (Carl Zeiss)
674 using a 40× objective lens.

675

Fluorescence *in situ* hybridization and immunofluorescence (FISH-IF)

charon:EGFP embryos at stages of interest were processed according to He et al., (2020) with minor modifications. Briefly, fixed embryos were permeabilized with 1% Triton X-100 in PBS for 1 hour and were hybridized with DIG-labelled probes at 60°C. Chromogenic reaction was performed with either TSA Plus Cyanine 3 Kit (Akoya Biosciences) for *nkx3.1* or ImmPACT Vector Red (Vector Laboratories) for the other genes. Afterward, embryos were subjected to immunostaining against EGFP using anti-GFP antibody (1/500, A11122, Invitrogen).

References

Agathon, A., Thisse, C. and Thisse, B. (2003). The molecular nature of the zebrafish tail organizer. *Nature* **424**, 448–452.

Alexander, J. and Stainier, D. Y. R. (1999). A molecular pathway leading to endoderm formation in zebrafish. *Curr. Biol.* **9**, 1147–1157.

Alexander, J., Rothenberg, M., Henry, G. L. and Stainier, D. Y. R. (1999). casanova plays an early and essential role in endoderm formation in zebrafish. *Dev. Biol.* **215**, 343–357.

Amack, J. D. (2021). Cellular dynamics of EMT: lessons from live in vivo imaging of embryonic development. *Cell Commun. Signal.* **19**, 1–16.

Amack, J. D., Wang, X. and Yost, H. J. (2007). Two T-box genes play independent and cooperative roles to regulate morphogenesis of ciliated Kupffer's vesicle in zebrafish. *Dev. Biol.* **310**, 196–210.

Barresi, M. J. F., D'Angelo, J. A., Hernández, L. P. and Devoto, S. H. (2001). Distinct mechanisms regulate slow-muscle development. *Curr. Biol.* **11**, 1432–1438.

Beck, C. W. (2015). Development of the vertebrate tailbud. *Wiley Interdiscip. Rev. Dev. Biol.* **4**, 33–44.

Blum, M., Feistel, K., Thumberger, T. and Schweickert, A. (2014). The evolution and conservation of left-right patterning mechanisms. *Development* **141**, 1603–1613.

Brennan, J., Norris, D. P. and Robertson, E. J. (2002). Nodal activity in the node governs left-right asymmetry. *Genes Dev.* **16**, 2339–2344.

Brummett, A. R. and Dumont, J. N. (1978). Kupffer's vesicle in Fundulus heteroclitus: A scanning and transmission electron microscope study. *Tissue Cell* **10**, 11–22.

Campbell, B. C., Nabel, E. M., Murdock, M. H., Lao-Peregrin, C., Tsoulfas, P., Blackmore, M. G., Lee, F. S., Liston, C., Morishita, H. and Petsko, G. A. (2020). mGreenLantern: a bright monomeric fluorescent protein with rapid expression and cell filling properties for neuronal imaging. *Proc. Natl. Acad. Sci. U. S. A.* **117**, 30710–30721.

Caron, A., Xu, X. and Lin, X. (2012). Wnt/β-catenin signaling directly regulates Foxj1 expression and ciliogenesis in zebrafish Kupffer's vesicle. *Development* **139**, 514–524.

Chen, Y. Y., Harris, M. P., Levesque, M. P., Nüsslein-Volhard, C. and Sonawane, M. (2012). Heterogeneity across the dorso-ventral axis in zebrafish EVL is

regulated by a novel module consisting of sox, snail1a and max genes. *Mech. Dev.* **129**, 13–23.

Chertkova, A. O., Mastop, M., Postma, M., van Bommel, N., van der Niet, S., Batenburg, K. L., Joosen, L., Gadella, T. W. J., Okada, Y. and Goedhart, J. (2017). Robust and Bright Genetically Encoded Fluorescent Markers for Highlighting Structures and Compartments in Mammalian Cells. *bioRxiv*.

Compagnon, J., Barone, V., Rajshekar, S., Kottmeier, R., Pranjic-Ferscha, K., Behrndt, M. and Heisenberg, C. P. (2014). The notochord breaks bilateral symmetry by controlling cell shapes in the zebrafish laterality organ. *Dev. Cell* **31**, 774–783.

Cooper, M. S. and D'Amico, L. A. (1996). A cluster of noninvoluting endocytic cells at the margin of the zebrafish blastoderm marks the site of embryonic shield formation. *Dev. Biol.* **180**, 184–198.

Cortés, F., Daggett, D., Bryson-Richardson, R. J., Neyt, C., Maule, J., Gautier, P., Hollway, G. E., Keenan, D. and Currie, P. D. (2003). Cadherin-mediated differential cell adhesion controls slow muscle cell migration in the developing zebrafish myotome. *Dev. Cell* **5**, 865–876.

Devoto, S. H., Melançon, E., Eisen, J. S. and Westerfield, M. (1996). Identification

of separate slow and fast muscle precursor cells in vivo, prior to somite formation. *Development* **122**, 3371–3380.

Dheen, T., Sleptsova-Friedrich, I., Xu, Y., Clark, M., Lehrach, H., Gong, Z. and Korzh, V. (1999). Zebrafish tbx-c functions during formation of midline structures. *Development* **126**, 2703–2713.

Du, S. J. and Dienhart, M. (2001). Zebrafish tiggy-winkle hedgehog promoter directs notochord and floor plate green fluorescence protein expression in transgenic zebrafish embryos. *Dev. Dyn.* **222**, 655–666.

Elmore, S. (2007). Apoptosis: A Review of Programmed Cell Death. *Toxicol. Pathol.* **35**, 495–516.

Essner, J. J., Amack, J. D., Nyholm, M. K., Harris, E. B. and Yost, H. J. (2005). Kupffer's vesicle is a ciliated organ of asymmetry in the zebrafish embryo that initiates left-right development of the brain, heart and gut. *Development* **132**, 1247–1260.

Fabian, P., Tseng, K., Smeeton, J., Lancman, J. J., Dong, P. D. S., Cerny, R. and Crump, J. G. (2020). Lineage analysis reveals an endodermal contribution to the vertebrate pituitary. *Science (80-.).* **370**, 463–467.

Fu, Z., Peng, D., Zhang, M., Xue, F., Zhang, R., He, W., Xu, T. and Xu, P. (2020).

mEosEM withstands osmium staining and Epon embedding for super-resolution CLEM. *Nat. Methods* **17**, 55–58.

Gjorevski, N., Boghaert, E. and Nelson, C. M. (2012). Regulation of Epithelial-Mesenchymal Transition by Transmission of Mechanical Stress through Epithelial Tissues. *Cancer Microenviron.* **5**, 29–38.

Gourronc, F., Ahmad, N., Nedza, N., Eggleston, T. and Rebagliati, M. (2007). Nodal activity around Kupffer's vesicle depends on the T-box transcription factors notail and spadetail and on Notch signaling. *Dev. Dyn.* **236**, 2131–2146.

Hammond, C. L., Hinits, Y., Osborn, D. P. S., Minchin, J. E. N., Tettamanti, G. and Hughes, S. M. (2007). Signals and myogenic regulatory factors restrict pax3 and pax7 expression to dermomyotome-like tissue in zebrafish. *Dev. Biol.* **302**, 504–521.

Hashimoto, H., Rebagliati, M., Ahmad, N., Muraoka, O., Kurokawa, T., Hibi, M. and Suzuki, T. (2004). The Cerberus/Dan-family protein Charon is a negative regulator of Nodal signaling during left-right patterning in zebrafish. *Development* **131**, 1741–1753.

He, J., Mo, D., Chen, J. and Luo, L. (2020). Combined whole-mount fluorescence in situ hybridization and antibody staining in zebrafish embryos and larvae. *Nat.*

Protoc. **15**, 3361–3379.

Henrique, D., Abranches, E., Verrier, L. and Storey, K. G. (2015). Neuromesodermal progenitors and the making of the spinal cord. *Development* **142**, 2864–2875.

Hochgreb-Hägele, T., Yin, C., Koo, D. E. S., Bronner, M. E. and Stainier, D. Y. R. (2013). Laminin β1a controls distinct steps during the establishment of digestive organ laterality. *Development* **140**, 2734–2745.

Hojo, M., Takashima, S., Kobayashi, D., Sumeragi, A., Shimada, A., Tsukahara, T., Yokoi, H., Narita, T., Jindo, T., Kage, T., et al. (2007). Right-elevated expression of charon is regulated by fluid flow in medaka Kupffer's vesicle. *Dev. Growth Differ.* **49**, 395–405.

Hubaud, A. and Pourquié, O. (2014). Signalling dynamics in vertebrate segmentation. *Nat. Rev. Mol. Cell Biol.* **15**, 709–721.

Jopling, C., Boue, S. and Belmonte, J. C. I. (2011). Dedifferentiation, transdifferentiation and reprogramming: three routes to regeneration. *Nat. Rev. Mol. Cell Biol.* **12**, 79–89.

Joseph, E. M. and Cassetta, L. A. (1999). Mespo: a novel basic helix-loop-helix gene expressed in the presomitic mesoderm and posterior tailbud of Xenopus embryos.

Mech. Dev. **82**, 191–194.

Kikuchi, Y., Agathon, A., Alexander, J., Thisse, C., Waldron, S., Yelon, D., Thisse, B. and Stainier, D. Y. R. (2001). casanova encodes a novel Sox-related protein necessary and sufficient for early endoderm formation in zebrafish. *Genes Dev.* **15**, 1493–1505.

Kikuta, H. and Kawakami, K. (2009). Transient and Stable Transgenesis Using Tol2 Transposon Vectors. In *Zebrafish: Methods and Protocols* (ed. Lieschke, G. J.), Oates, A. C.), and Kawakami, K.), pp. 69–84. Totowa, NJ: Humana Press.

Kimmel, C. B., Ballard, W. W., Kimmel, S. R., Ullmann, B. and Schilling, T. F. (1995). Stages of embryonic development of the zebrafish. *Dev. Dyn.* **203**, 253–310.

Kupffer, C. (1868). Beobachtungen fiber die Entwicklung. *Anatomie* 209–272.

Long, S., Ahmad, N. and Rebagliati, M. (2003). The zebrafish nodal-related gene southpaw is required for visceral and diencephalic left-right asymmetry. *Development* **130**, 2303–2316.

Lopes, S. S., Lourenço, R., Pacheco, L., Moreno, N., Kreiling, J. and Saúde, L. (2010). Notch signalling regulates left-right asymmetry through ciliary length control. *Development* **137**, 3625–3632.

Ma, R. C., Jacobs, C. T., Sharma, P., Kocha, K. M. and Huang, P. (2018). Stereotypic generation of axial tenocytes from bipartite sclerotome domains in zebrafish. *PLoS Genet.* **14**, 1–29.

Marques, S., Borges, A. C., Silva, A. C., Freitas, S., Cordenonsi, M. and Belo, J. A. (2004). The activity of the Nodal antagonist Cerl-2 in the mouse node is required for correct L/R body axis. *Genes Dev.* **18**, 2342–2347.

Matsui, T., Ishikawa, H. and Bessho, Y. (2015). Cell collectivity regulation within migrating cell cluster during Kupffer's vesicle formation in zebrafish. *Front. Cell Dev. Biol.* **3**, 27.

Melby, A. E., Warga, R. M. and Kimmel, C. B. (1996). Specification of cell fates at the dorsal margin of the zebrafish gastrula. *Development* **122**, 2225–2237.

Merrell, A. J. and Stanger, B. Z. (2016). Adult cell plasticity in vivo: De-differentiation and transdifferentiation are back in style. *Nat. Rev. Mol. Cell Biol.* **17**, 413–425.

Minegishi, K., Rothé, B., Komatsu, K. R., Ono, H., Ikawa, Y., Nishimura, H., Katoh, T. A., Kajikawa, E., Sai, X., Miyashita, E., et al. (2021). Fluid flow-induced left-right asymmetric decay of Dand5 mRNA in the mouse embryo requires a Bicc1-Ccr4 RNA degradation complex. *Nat. Commun.* **12**, 4071.

Mizoguchi, T., Verkade, H., Heath, J. K., Kuroiwa, A. and Kikuchi, Y. (2008). Sdf1/Cxcr4 signaling controls the dorsal migration of endodermal cells during zebrafish gastrulation. *Development* **135**, 2521–2529.

Molina, G. A., Watkins, S. C. and Tsang, M. (2007). Generation of FGF reporter transgenic zebrafish and their utility in chemical screens. *BMC Dev. Biol.* **7**, 1–14.

Montague, T. G., Gagnon, J. A. and Schier, A. F. (2018). Conserved regulation of Nodal-mediated left-right patterning in zebrafish and mouse. *Development* **145**, dev171090.

Moriyama, Y., Kawanishi, T., Nakamura, R., Tsukahara, T., Sumiyama, K., Suster, M. L., Kawakami, K., Toyoda, A., Fujiyama, A., Yasuoka, Y., et al. (2012). The medaka zic1/zic4 mutant provides molecular insights into teleost caudal fin evolution. *Curr. Biol.* **22**, 601–607.

Mosimann, C., Panáková, D., Werdich, A. A., Musso, G., Burger, A., Lawson, K. L., Carr, L. A., Nevis, K. R., Sabeh, M. K., Zhou, Y., et al. (2015). Chamber identity programs drive early functional partitioning of the heart. *Nat. Commun.* **6**, 8146.

Nakamura, T., Saito, D., Kawasumi, A., Shinohara, K., Asai, Y., Takaoka, K., Dong, F., Takamatsu, A., Belo, J. A., Mochizuki, A., et al. (2012). Fluid flow

and interlinked feedback loops establish left–right asymmetric decay of Cerl2 mRNA. *Nat. Commun.* **3**, 1322.

Oteíza, P., Köppen, M., Concha, M. L. and Heisenberg, C. P. (2008). Origin and shaping of the laterality organ in zebrafish. *Development* **135**, 2807–2813.

Paez-Segala, M. G., Sun, M. G., Shtengel, G., Viswanathan, S., Baird, M. A., Macklin, J. J., Patel, R., Allen, J. R., Howe, E. S., Piszczek, G., et al. (2015). Fixation-resistant photoactivatable fluorescent proteins for CLEM. *Nat. Methods* **12**, 215–218.

Plein, A., Fantin, A., Denti, L., Pollard, J. W. and Ruhrberg, C. (2018). Erythro-myeloid progenitors contribute endothelial cells to blood vessels. *Nature* **562**, 223–228.

Prummel, K. D., Hess, C., Nieuwenhuize, S., Parker, H. J., Rogers, K. W., Kozmikova, I., Racioppi, C., Brombacher, E. C., Czarkwiani, A., Knapp, D., et al. (2019). A conserved regulatory program initiates lateral plate mesoderm emergence across chordates. *Nat. Commun.* **10**, 1–15.

Rembold, M., Lahiri, K., Foulkes, N. S. and Wittbrodt, J. (2006). Transgenesis in fish: Efficient selection of transgenic fish by co-injection with a fluorescent reporter construct. *Nat. Protoc.* **1**, 1133–1139.

865 **Row, R. H. and Kimelman, D.** (2009). Bmp inhibition is necessary for post-
866 gastrulation patterning and morphogenesis of the zebrafish tailbud. *Dev. Biol.* **329**,
867 55–63.
868 **Row, R. H., Tsotras, S. R., Goto, H. and Martin, B. L.** (2015). The zebrafish tailbud
869 contains two independent populations of midline progenitor cells that maintain
870 long-term germ layer plasticity and differentiate based on local signaling cues.
871 *Development* **143**, 244–254.
872 **Sakaguchi, T., Kikuchi, Y., Kuroiwa, A., Takeda, H. and Stainier, D. Y. R.** (2006).
873 The yolk syncytial layer regulates myocardial migration by influencing
874 extracellular matrix assembly in zebrafish. *Development* **133**, 4063–4072.
875 **Sambasivan, R. and Steventon, B.** (2021). Neuromesodermal Progenitors: A Basis for
876 Robust Axial Patterning in Development and Evolution. *Front. Cell Dev. Biol.* **8**,
877 1–9.
878 **Schindelin, J., Arganda-Carreras, I., Frise, E., Kaynig, V., Longair, M., Pietzsch,**
879 **T., Preibisch, S., Rueden, C., Saalfeld, S., Schmid, B., et al.** (2012). Fiji: An
880 open-source platform for biological-image analysis. *Nat. Methods* **9**, 676–682.
881 **Schulte-Merker, S., van Eeden, F. J., Halpern, M. E., Kimmel, C. B. and Nusslein-**
882 **Volhard, C.** (1994). no tail (ntl) is the zebrafish homologue of the mouse T

(Brachyury) gene. *Development* **120**, 1009–1015.

Scott, A. and Stemple, D. L. (2004). Zebrafish Notochordal Basement Membrane: Signaling and Structure. *Curr. Top. Dev. Biol.* **65**, 229–253.

Shimada, A., Kawanishi, T., Kaneko, T., Yoshihara, H., Yano, T., Inohaya, K., Kinoshita, M., Kamei, Y., Tamura, K. and Takeda, H. (2013). Trunk exoskeleton in teleosts is mesodermal in origin. *Nat. Commun.* **4**, 1638–1639.

Shook, D. R., Majer, C. and Keller, R. (2004). Pattern and morphogenesis of presumptive superficial mesoderm in two closely related species, Xenopus laevis and Xenopus tropicalis. *Dev. Biol.* **270**, 163–185.

Stickney, H. L., Barresi, M. J. F. and Devoto, S. H. (2000). Somite development in Zebrafish. *Dev. Dyn.* **219**, 287–303.

Stratman, A. N., Pezoa, S. A., Farrelly, O. M., Castranova, D., Dye, L. E., Butler, M. G., Sidik, H., Talbot, W. S. and Weinstein, B. M. (2017). Mural-Endothelial cell-cell interactions stabilize the developing zebrafish dorsal aorta. *Development* **144**, 115–127.

Tsutsui, H., Karasawa, S., Shimizu, H., Nukina, N. and Miyawaki, A. (2005). Semi-rational engineering of a coral fluorescent protein into an efficient highlighter. *EMBO Rep.* **6**, 233–238.

Warga, R. M. and Kane, D. A. (2018). Wilson cell origin for kupffer's vesicle in the zebrafish. *Dev. Dyn.* **247**, 1057–1069.

Xiong, F., Ma, W., Hiscock, T. W., Mosaliganti, K. R., Tentner, A. R., Brakke, K. A., Rannou, N., Gelas, A., Souhait, L., Swinburne, I. A., et al. (2014). Interplay of cell shape and division orientation promotes robust morphogenesis of developing epithelia. *Cell* **159**, 415–427.

Yang, J. and Weinberg, R. A. (2008). Epithelial-Mesenchymal Transition: At the Crossroads of Development and Tumor Metastasis. *Dev. Cell* **14**, 818–829.

Yang, J., Antin, P., Berx, G., Blanpain, C., Brabletz, T., Bronner, M., Campbell, K., Cano, A., Casanova, J., Christofori, G., et al. (2020). Guidelines and definitions for research on epithelial–mesenchymal transition. *Nat. Rev. Mol. Cell Biol.* **21**, 341–352.

Yoo, K. W., Kim, C. H., Park, H. C., Kim, S. H., Kim, H. S., Hong, S. K., Han, S., Rhee, M. and Huh, T. L. (2003). Characterization and expression of a presomitic mesoderm-specific mespo gene in zebrafish. *Dev. Genes Evol.* **213**, 203–206.

Yoon, J. K., Moon, R. T. and Wold, B. (2000). The bHLH class protein pMesogeninl can specify paraxial mesoderm phenotypes. *Dev. Biol.* **222**, 376–391.

Zhang, J., Jiang, Z., Liu, X. and Meng, A. (2016). Eph-ephrin signaling maintains the

boundary of dorsal forerunner cell cluster during morphogenesis of the zebrafish embryonic left-right organizer. *Development* **143**, 2603–2615.

Figure 1

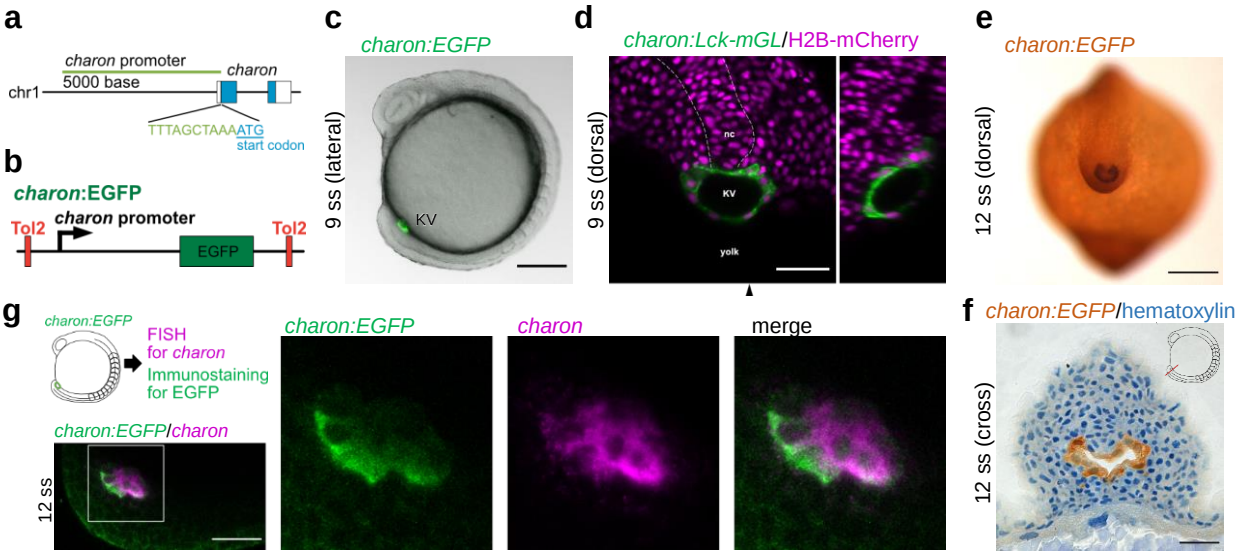

Figure 2

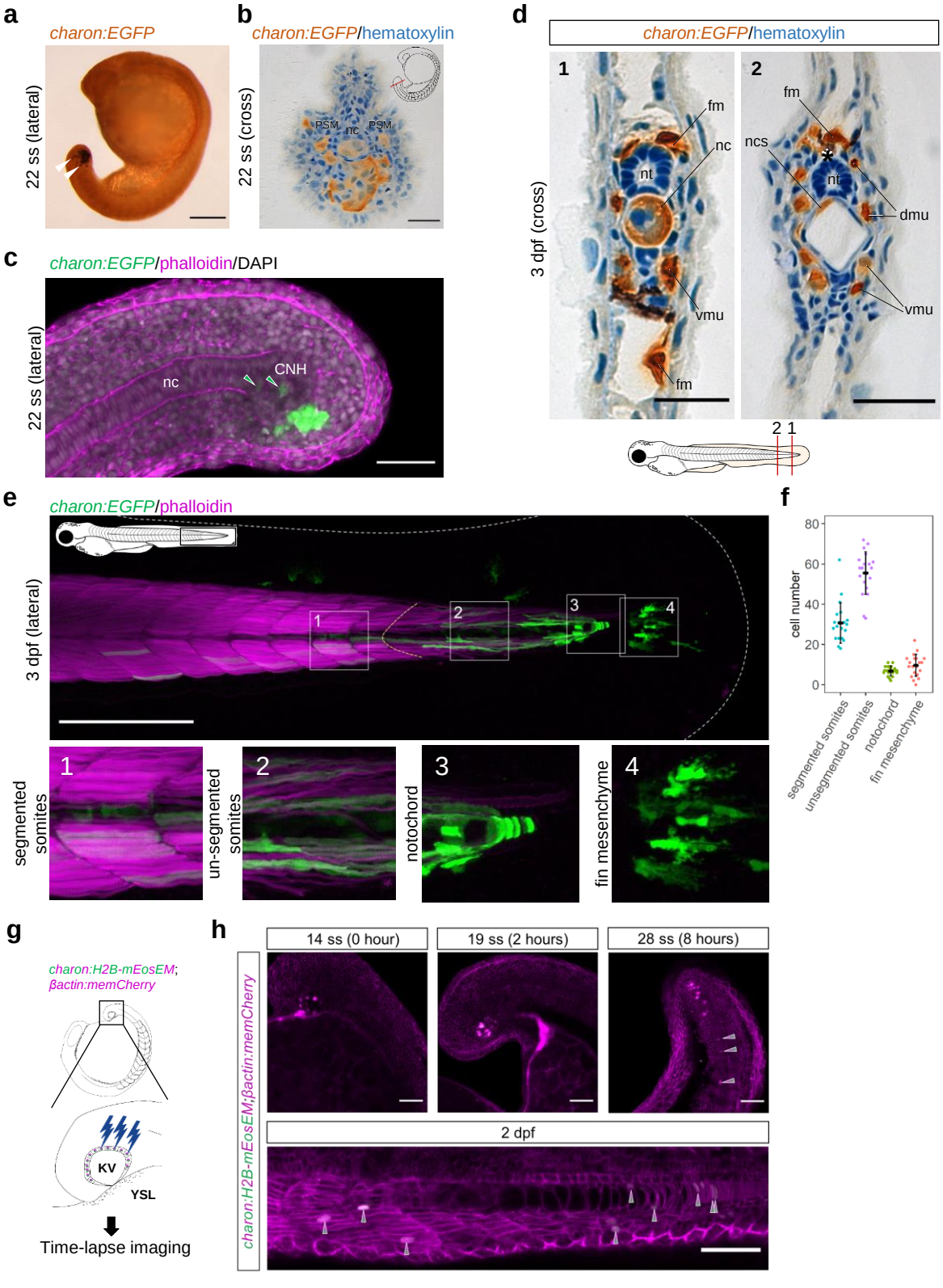

Figure 3

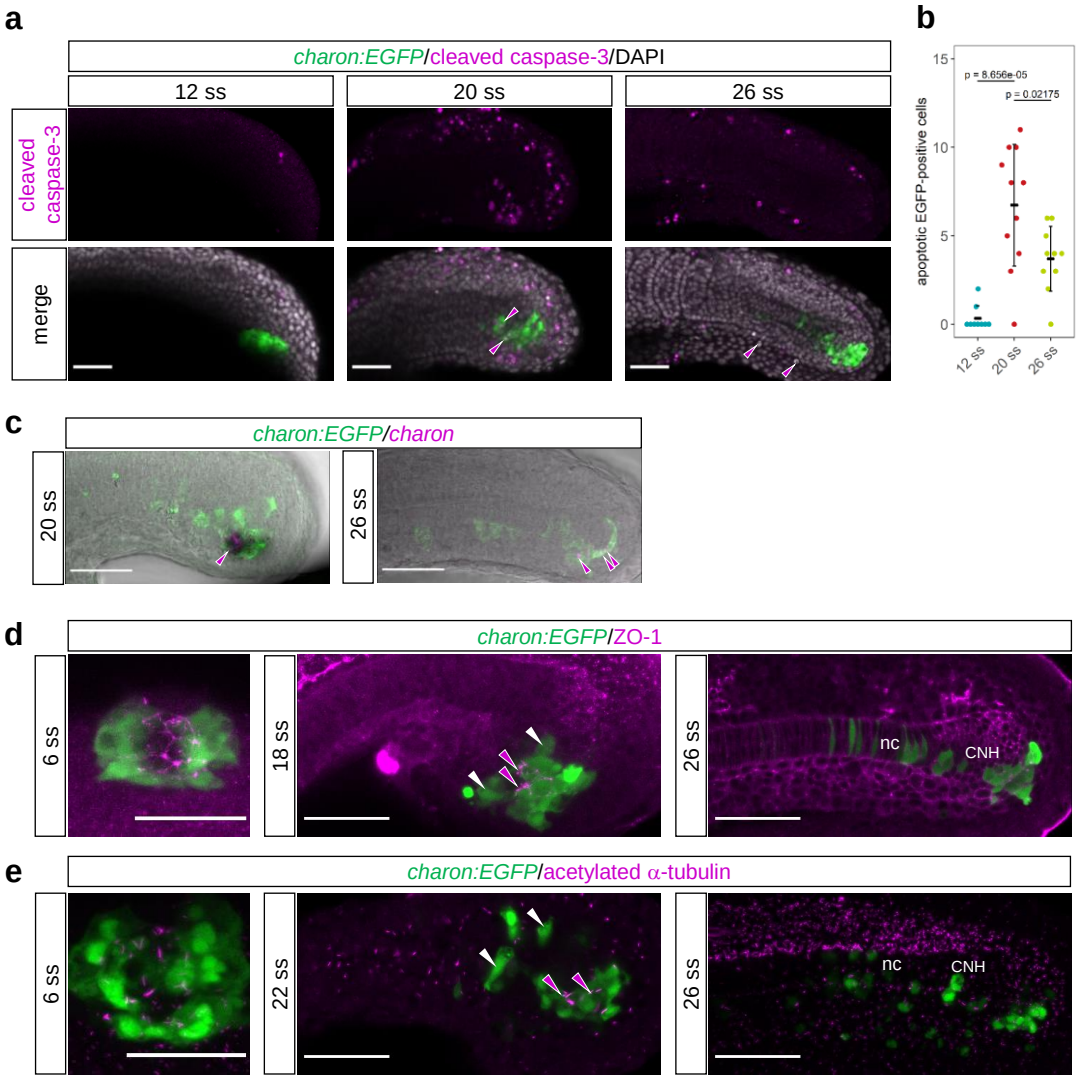

Figure 4

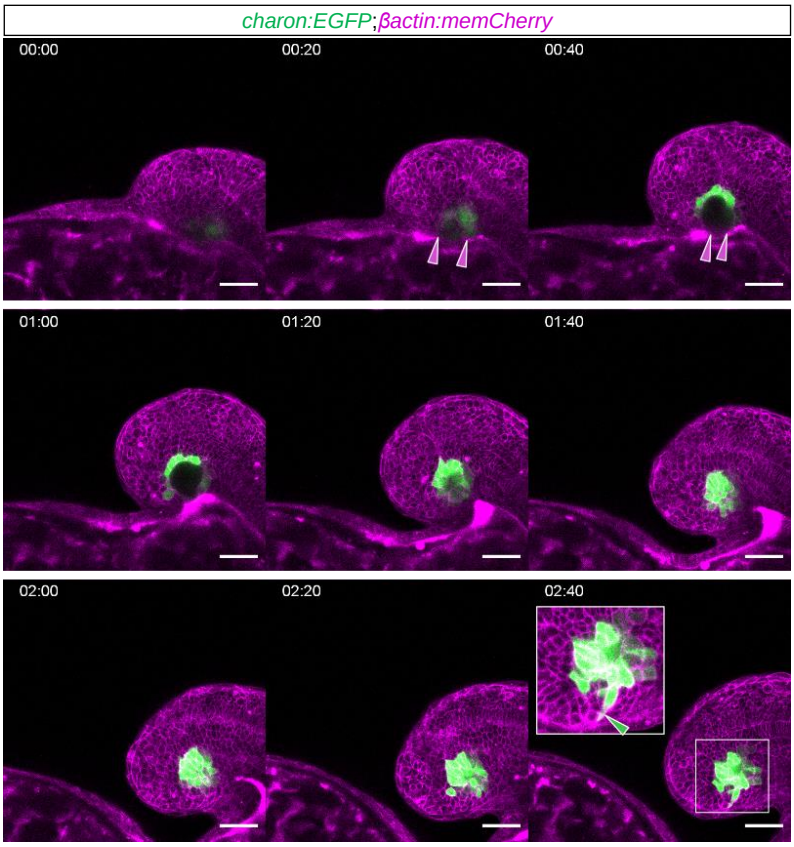

Figure 5

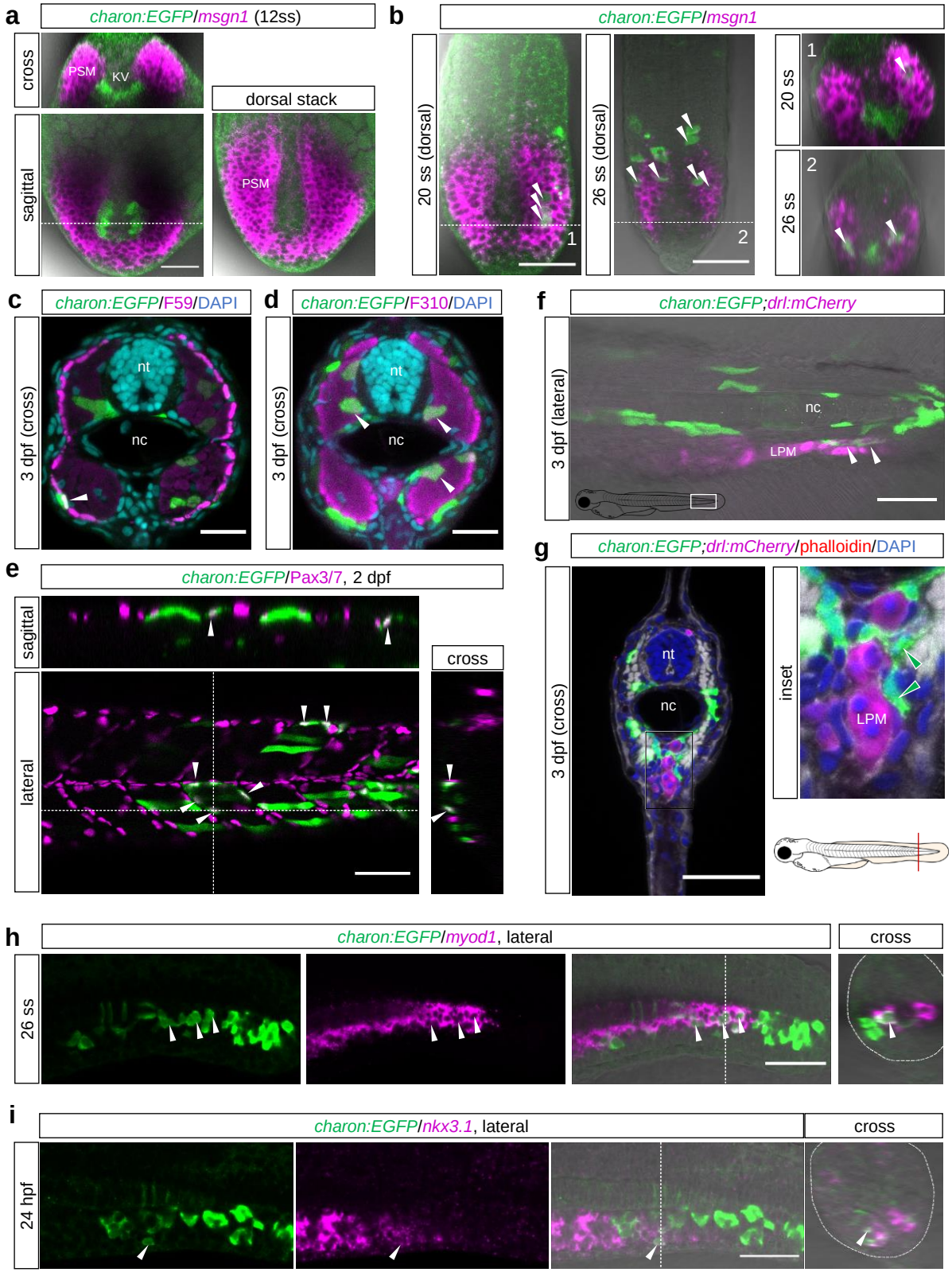

Figure 6

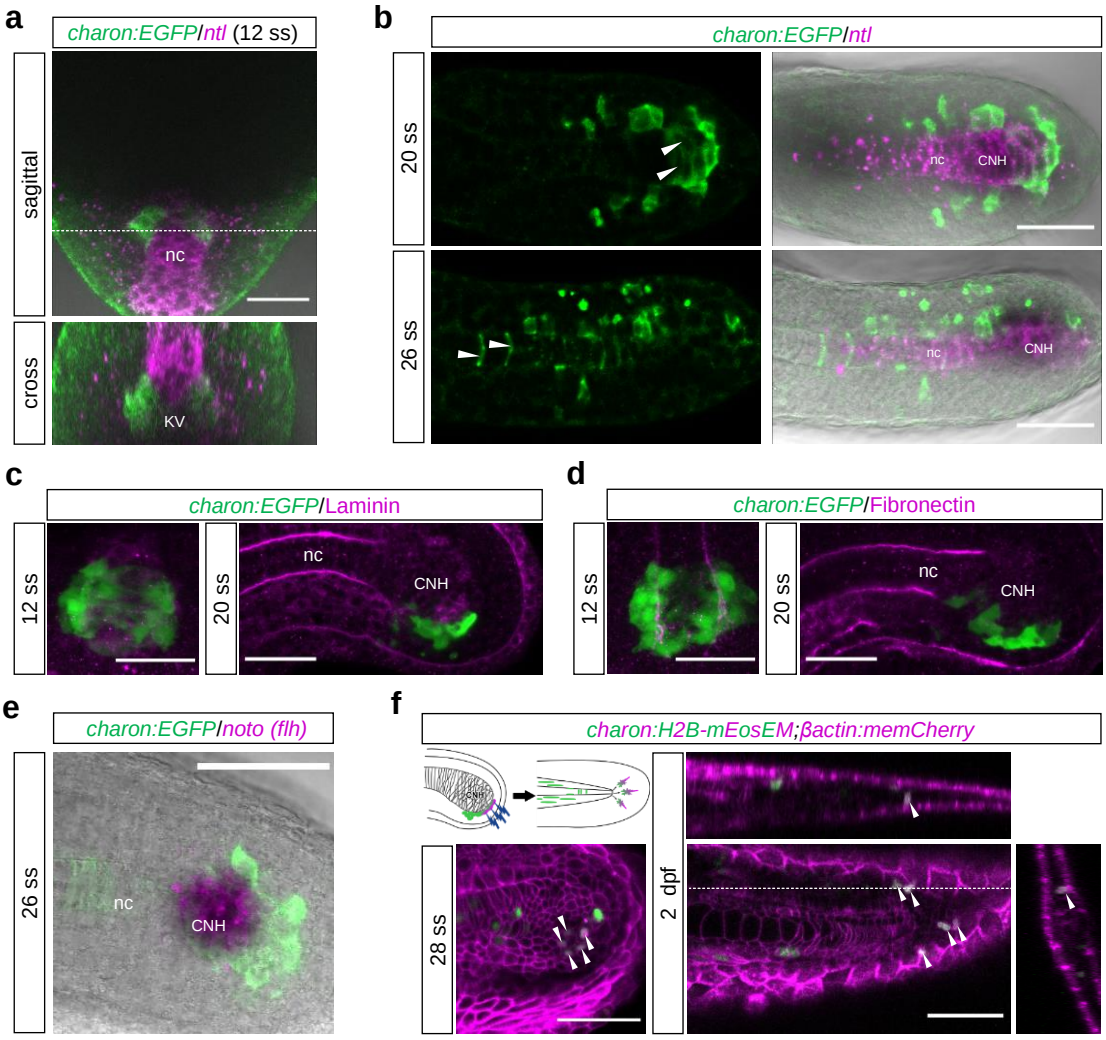

Figure 7

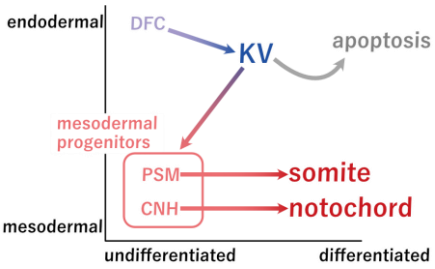

Supplementary Figure 1

Supplementary Figure 2

Supplementary Figure 3

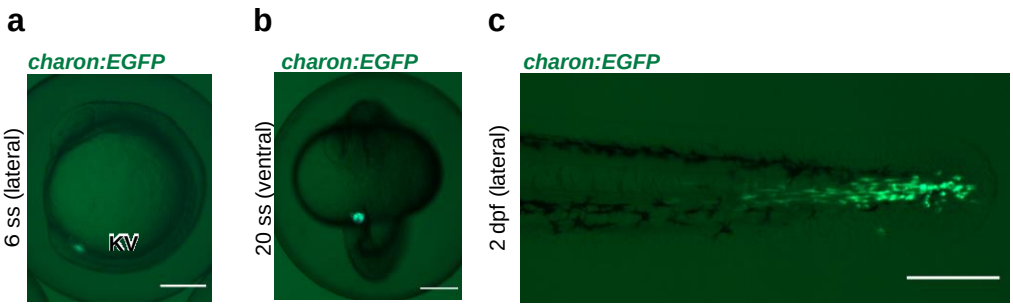

Supplementary Figure 4

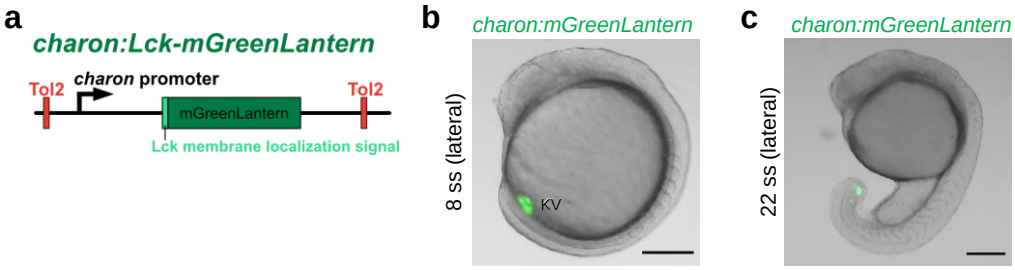

Supplementary Figure 5

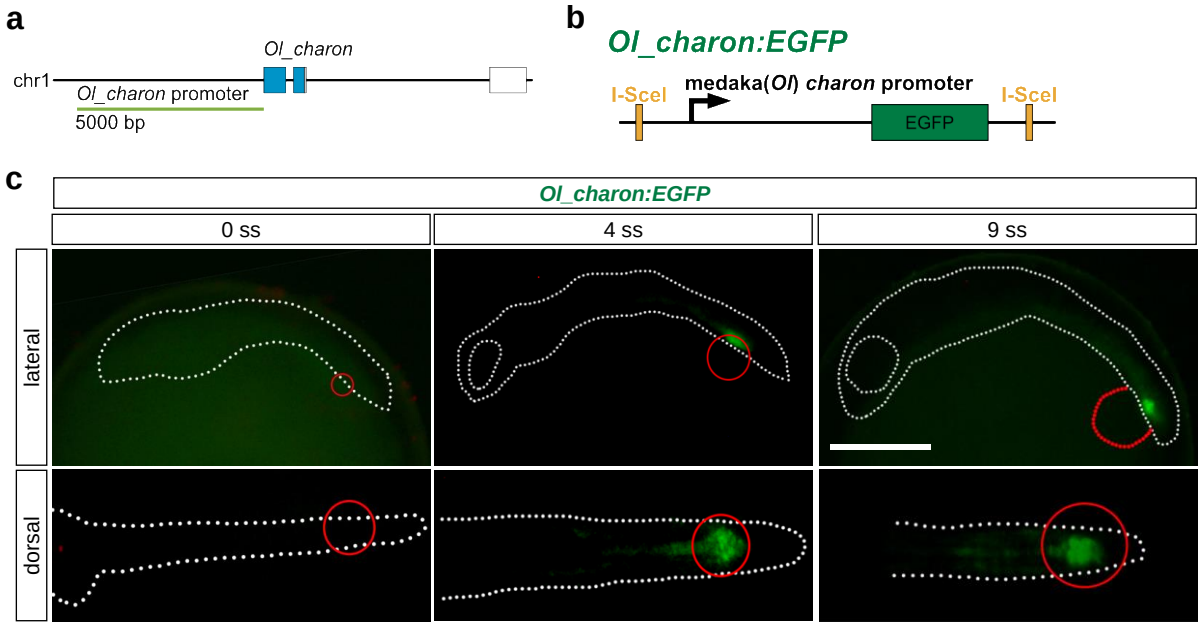

Supplementary Figure 6

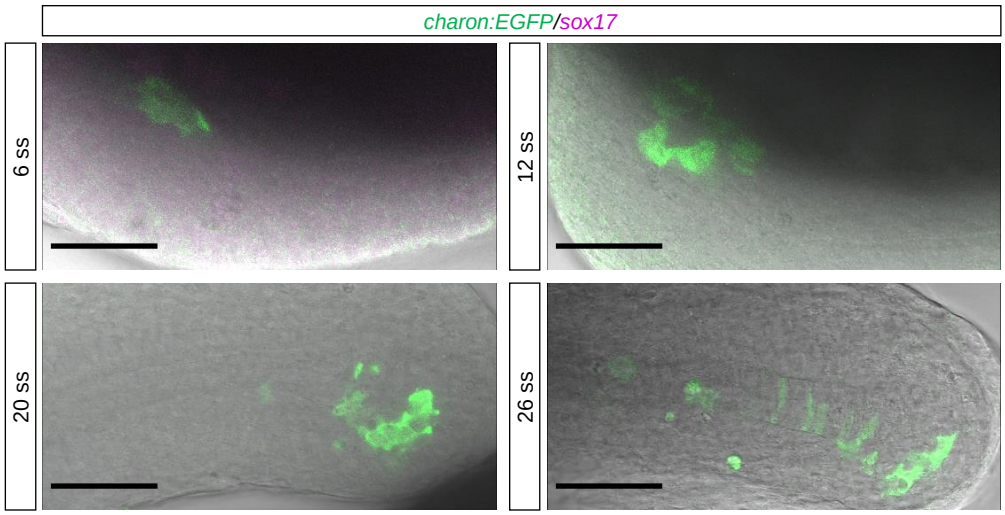

Supplementary Figure 7

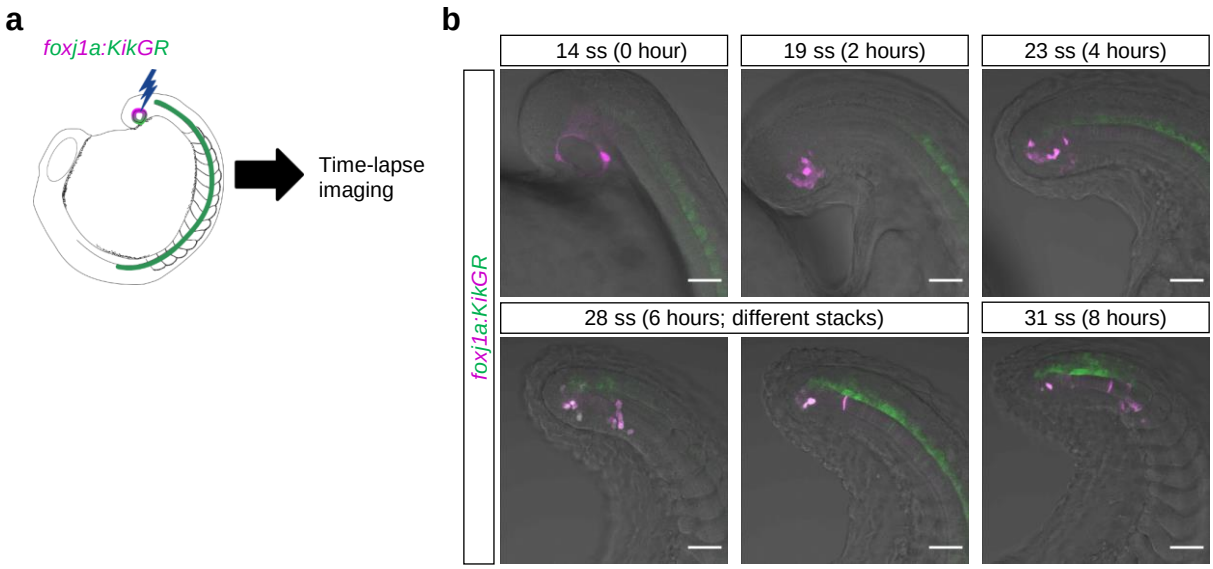

Supplementary Figure 8